

ARTICLE

Open Access

# Broad ultra-potent neutralization of SARS-CoV-2 variants by monoclonal antibodies specific to the tip of RBD

Hang Ma<sup>1</sup>, Yingying Guo<sup>2,3</sup>, Haoneng Tang<sup>1</sup>, Chien-Te K. Tseng<sup>4,5,6,7</sup>, Lei Wang<sup>1</sup>, Huifang Zong<sup>1</sup>, Zhenyu Wang<sup>8</sup>, Yang He<sup>8</sup>, Yunsong Chang<sup>8</sup>, Shusheng Wang<sup>9</sup>, Haiqiu Huang<sup>9</sup>, Yong Ke<sup>1</sup>, Yunsheng Yuan<sup>1</sup>, Mingyuan Wu<sup>1</sup>, Yuanyuan Zhang<sup>2,3</sup>, Aleksandra Drelich<sup>4</sup>, Kempaiah Rayavara Kempaiah<sup>4</sup>, Bi-Hung Peng<sup>5</sup>, Ailin Wang<sup>9</sup>, Kaiyong Yang<sup>9</sup>, Haiyang Yin<sup>1</sup>, Junjun Liu<sup>1</sup>, Yali Yue<sup>1</sup>, Wenbo Xu<sup>10</sup>, Shuangli Zhu<sup>10</sup>, Tianjiao Ji<sup>10</sup>, Xiaoju Zhang<sup>11</sup>, Ziqi Wang<sup>11</sup>, Gang Li<sup>8</sup>, Guangchun Liu<sup>8</sup>, Jingjing Song<sup>8</sup>, Lingling Mu<sup>8</sup>, ZongShang Xiang<sup>8</sup>, Zhangyi Song<sup>9</sup>, Hua Chen<sup>9</sup>, Yanlin Bian<sup>1</sup>, Baohong Zhang<sup>1</sup>, Hui Chen<sup>1</sup>, Jiawei Zhang<sup>1</sup>, Yunji Liao<sup>1</sup>, Li Zhang<sup>9</sup>, Li Yang<sup>11</sup>, Yi Chen<sup>12</sup>, John Gilly<sup>8,9</sup>, Xiaodong Xiao<sup>8,9</sup>, Lei Han<sup>8,13</sup>, Hua Jiang<sup>8,9</sup>, Yueqing Xie<sup>9</sup> and Qiang Zhou<sup>2,3</sup> and Jianwei Zhu<sup>1,8,9,13</sup>

## Abstract

Severe acute respiratory syndrome coronavirus 2 (SARS-CoV-2) variants of concern (VOCs) continue to wreak havoc across the globe. Higher transmissibility and immunologic resistance of VOCs bring unprecedented challenges to epidemic extinguishment. Here we describe a monoclonal antibody, 2G1, that neutralizes all current VOCs and has surprising tolerance to mutations adjacent to or within its interaction epitope. Cryo-electron microscopy structure showed that 2G1 bound to the tip of receptor binding domain (RBD) of spike protein with small contact interface but strong hydrophobic effect, which resulted in nanomolar to sub-nanomolar affinities to spike proteins. The epitope of 2G1 on RBD partially overlaps with angiotensin converting enzyme 2 (ACE2) interface, which enables 2G1 to block interaction between RBD and ACE2. The narrow binding epitope but high affinity bestow outstanding therapeutic efficacy upon 2G1 that neutralized VOCs with sub-nanomolar half maximal inhibitory concentration in vitro. In SARS-CoV-2, Beta or Delta variant-challenged transgenic mice and rhesus macaque models, 2G1 protected animals from clinical illness and eliminated viral burden, without serious impact to animal safety. Mutagenesis experiments suggest that 2G1 is potentially capable of dealing with emerging SARS-CoV-2 variants in the future. This report characterized the therapeutic antibodies specific to the tip of spike against SARS-CoV-2 variants and highlights the potential clinical applications as well as for developing vaccine and cocktail therapy.

Correspondence: Lei Han (lei.han@jchobio.com) or Hua Jiang (hua.jiang@jcholabs.com) or Yueqing Xie (yueqing.xie@jcholabs.com) or Qiang Zhou (zhouqiang@westlake.edu.cn) or Jianwei Zhu (jianweiz@sjtu.edu.cn)

<sup>1</sup>Engineering Research Center of Cell and Therapeutic Antibody, Ministry of Education, China; School of Pharmacy, Shanghai Jiao Tong University, Shanghai, China

<sup>2</sup>Center for Infectious Disease Research, Westlake Laboratory of Life Sciences and Biomedicine, Key Laboratory of Structural Biology of Zhejiang, School of Life Sciences, Westlake University, Hangzhou, Zhejiang, China

Full list of author information is available at the end of the article

These authors contributed equally: Hang Ma, Yingying Guo, Haoneng Tang, Chien-Te K. Tseng

## Introduction

Since the first Coronavirus Disease 2019 (COVID-19) case was diagnosed at the end of 2019, the severe acute respiratory syndrome coronavirus 2 (SARS-CoV-2) has caused more than 200 million confirmed infections and 4.5 million deaths in the following eighteen months, with no sign of stopping (<https://ourworldindata.org/coronavirus>)<sup>1–6</sup>. The hope-placed distribution of vaccines once appeared to effectively control the virus spread. However, the antigenic evolution of SARS-CoV-2,

© The Author(s) 2022



**Open Access** This article is licensed under a Creative Commons Attribution 4.0 International License, which permits use, sharing, adaptation, distribution and reproduction in any medium or format, as long as you give appropriate credit to the original author(s) and the source, provide a link to the Creative Commons license, and indicate if changes were made. The images or other third party material in this article are included in the article's Creative Commons license, unless indicated otherwise in a credit line to the material. If material is not included in the article's Creative Commons license and your intended use is not permitted by statutory regulation or exceeds the permitted use, you will need to obtain permission directly from the copyright holder. To view a copy of this license, visit <http://creativecommons.org/licenses/by/4.0/>.

especially in the spike (S) protein associated with receptor binding, alters the viral immunogenicity, facilitating the virus immune escape and crossing transmission barriers<sup>7,8</sup>.

Receptor binding domain (RBD) on the S protein is a determinant that mediates the binding of SARS-CoV-2 to the angiotensin converting enzyme 2 (ACE2). Neutralizing antibodies targeting RBD were proved to be effective<sup>9–11</sup>. Correspondingly, substitutions on RBD may reduce neutralizing efficacy<sup>12–14</sup>. Several variants, listed as Variant of Concern (VOC), featured with RBD substitutions and non-RBD mutations showed higher transmissibility and led to more severe illness<sup>15–17</sup>, which has been causing great global dissemination concern. SARS-CoV-2 B.1.1.7 (Alpha) was first identified in United Kingdom in late summer of 2020 and rapidly became the dominant variant. This variant has nine mutations in the S protein, one of which is N501Y in RBD<sup>18</sup>. Alpha variant possesses a comparative transmission advantage, with a reproductive number 50% to 100% higher than other non-VOC lineages<sup>1</sup>. Vaccine-elicited neutralizing antibody responses were shown to be at risk of being desensitized by Alpha<sup>19</sup>. SARS-CoV-2 B.1.351 (Beta) has three substitutions in RBD, i.e., K417N, E484K, and N501Y. Incorporation of E484K empowers variants possible complete resistance to plasma neutralization<sup>20</sup>. Mutation E484K together with K417N and N501Y largely contribute to the escape of Beta variant from convalescent and vaccine-induced sera<sup>21,22</sup>. SARS-CoV-2 P.1 (Gamma) shares three identical site mutations in RBD with Beta variant, and their differences are that the substitution of K417 is threonine in Gamma variant, while is asparagine in Beta variant. Similarly, Gamma variant notably reduced susceptibility to antibody treatment and vaccine protection<sup>23,24</sup>. SARS-CoV-2 B.1.617.2 (Delta) was first reported in India and quickly spread globally in the first half of 2021. This strain has more than ten S protein mutations and two of them, L452R and T478K, are in RBD. Delta variant exhibits more extensive immunologic resistance than Alpha, escaping from many S protein antibodies targeting RBD and non-RBD epitopes<sup>25,26</sup>. Individuals who recovered from Beta and Gamma variants are more susceptible to Delta infection<sup>27</sup>. In addition to these VOCs, potential outbreaks of several variants have raised public concern, such as the recently spreading variant C.37 (Lambda)<sup>28</sup> and the new variant B.1.621 (Mu)<sup>29</sup>. The emergence of these variants, even possible hybrid variants, raises the risk of compromising the therapeutic effectiveness of vaccines and neutralizing antibodies that were previously developed<sup>30,31</sup>.

Here we report our efforts on discovering neutralizing antibodies that provide extensive protection against the variants with global impact, especially the VOCs. We isolated RBD-positive single B cells from convalescent individuals and cloned monoclonal antibodies (mAbs). After a series of programmed screening, several mAbs

with remarkable neutralizing effect were panned out from the candidates (Fig. 1a). One of these antibodies, designated as 2G1, efficiently neutralized all VOCs including widely spread Alpha, Beta, Gamma, Delta variants and Cluster 5, a variant with Y453F substitution once caused public concern due to the zoonotic characteristics. The antibody 2G1 was subsequently fully characterized physico-chemically and biologically, as well as evaluated in potential clinical applications.

## Results

### Molecule discovery of 2G1

We collected blood samples from 20 convalescent individuals who were infected by SARS-CoV-2 in February 2020. Peripheral blood mononuclear cells (PBMCs) were enriched and sorted with fluorescently labeled recombinant SARS-CoV-2 RBD (WA1/2020) protein (Fig. 1b). Over 1200 B cells were isolated and more than 500 pairs of IgG antibody genes were cloned by single-cell polymerase chain reaction (PCR). Of which, 375 are kappa subtype and 174 are lambda subtype (Fig. 1c). 143 RBD binders were obtained after the enzyme-linked immunosorbent assay (ELISA)-based preliminary screening (Fig. 1d). In the following pseudovirus-based screening, three molecules, including 2G1, displayed ultra-potent neutralization with half maximal inhibitory concentration ( $IC_{50}$ ) less than 0.01  $\mu\text{g}/\text{mL}$  (Fig. 1e). Antibody 2G1 stood out from these candidates after further investigation despite that its binding and ACE2 blocking abilities were not remarkable (Supplementary Fig. S1a, b). In the germline analysis of 33 candidates, 23 heavy chains were from IGHV3 and 18 light chains were from IGKV1 (Supplementary Fig. S2a). Six heavy chains, including 2G1, were from IGHV3-53, which was reported to have short complementarity-determining region with minimal affinity but high efficacy (Supplementary Fig. S2b)<sup>32</sup>.

WA1/2020 RBD-mFc and S trimer proteins and pseudovirus were employed to further confirm the antigen-binding and neutralizing ability of 2G1. Antibody 2G1 bound to RBD-mFc and S trimer with half maximal effective concentration ( $EC_{50}$ ) of 0.016  $\mu\text{g}/\text{mL}$  and 0.135  $\mu\text{g}/\text{mL}$ , respectively (Fig. 2a, b) and neutralized WA1/2020 pseudovirus with  $IC_{50}$  0.0031  $\mu\text{g}/\text{mL}$  (Fig. 2c), in line with the results of previous screening. Affinity of monovalent 2G1 (Fab) to RBD was measured by surface plasmon resonance (SPR). Relatively moderate dissociation constant ( $K_d$ ) of 2G1 to WA1/2020 RBD was determined as  $1.05 \times 10^{-3}/\text{s}$ . The rapid binding of 2G1 with association constant ( $K_a$ ) =  $2.55 \times 10^6/\text{Ms}$  offered a subnanomolar equilibrium dissociation constant ( $K_D$ ) value of 0.41 nM (Fig. 2d). Next, the antibody 2G1 was moved to further characterization including in vitro and in vivo biological activities as well as structural and mechanism investigation.

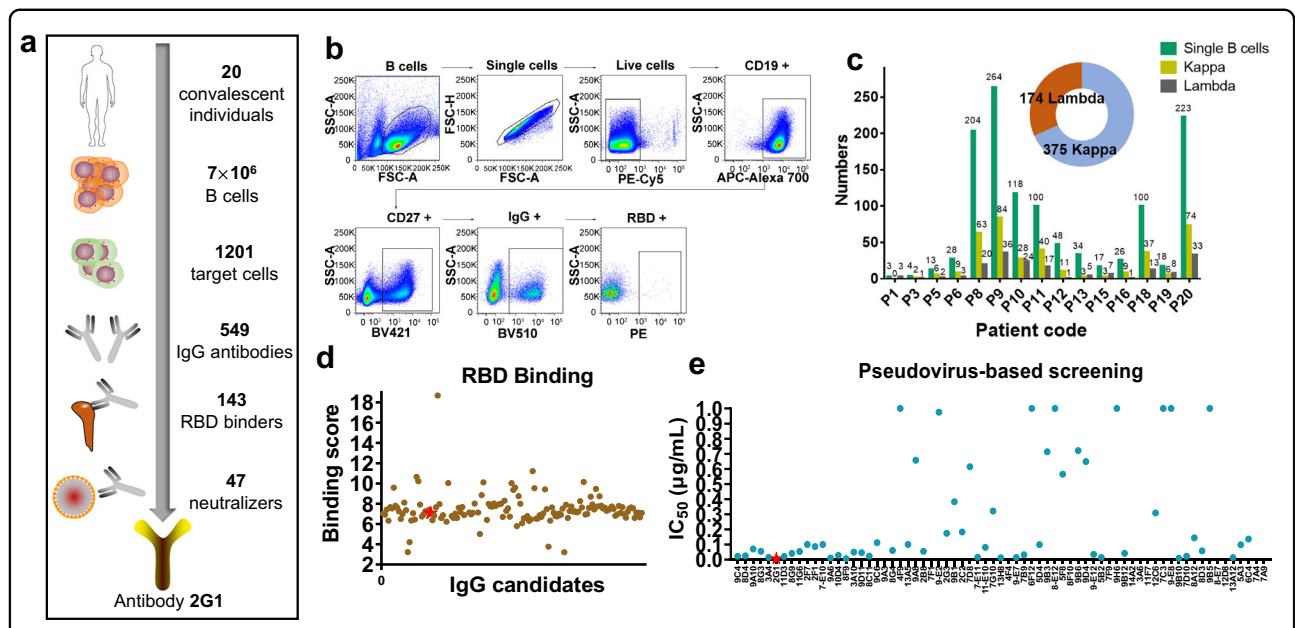


**Fig. 1 Cell isolation, antibody cloning, and candidate panning.** **a** Isolation strategy of highly potent neutralizing antibodies as depicted by a diagram. **b** RBD-specific B cells were isolated from convalescent subjects of SARS-CoV-2 infection by fluorescence-activated cell sorting. The 7ADD<sup>+</sup>/CD19<sup>+</sup>/CD27<sup>+</sup>/IgG<sup>+</sup>/RBD<sup>+</sup> gate is shown and highlighted in the boxes. **c** Statistics of the number of paired antibodies from each subject, as well as the number of kappa and lambda subtypes. **d** Binding scores of antibody candidates against SARS-CoV-2 RBD as measured by ELISA and scores higher than 2 are presented. 2G1 is highlighted in red. **e** Candidate panning using a WA1/2020 pseudovirus-based screening model. Antibodies were 10-fold serially diluted from 10<sup>1</sup> µg/mL to 10<sup>-4</sup> µg/mL.

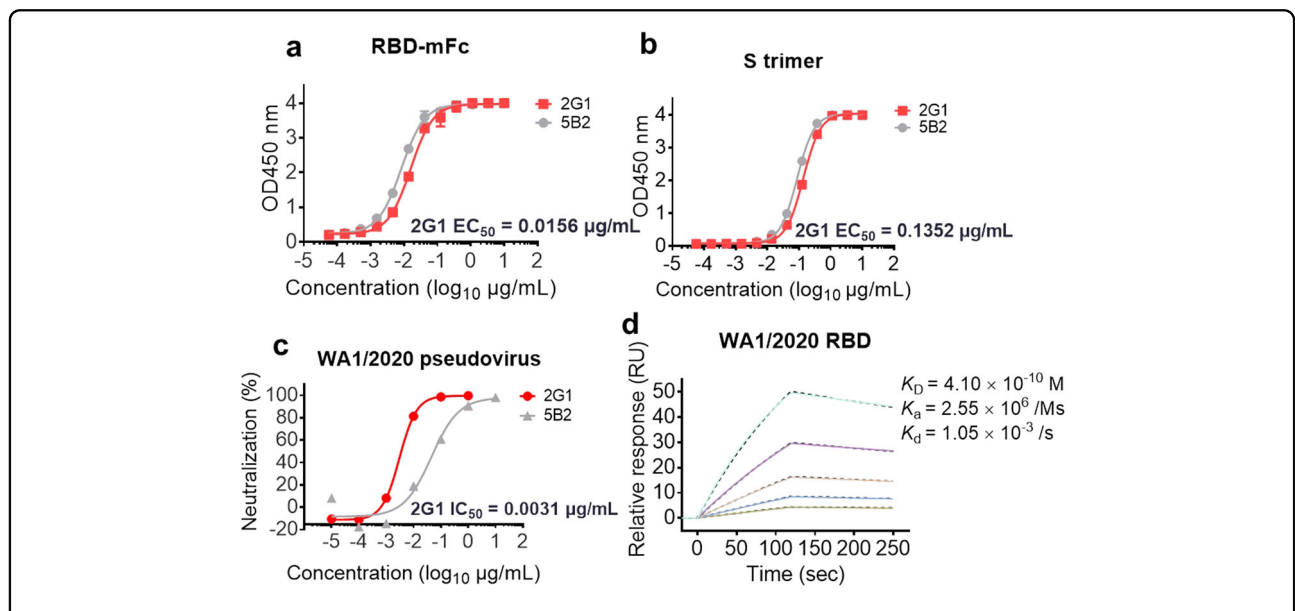
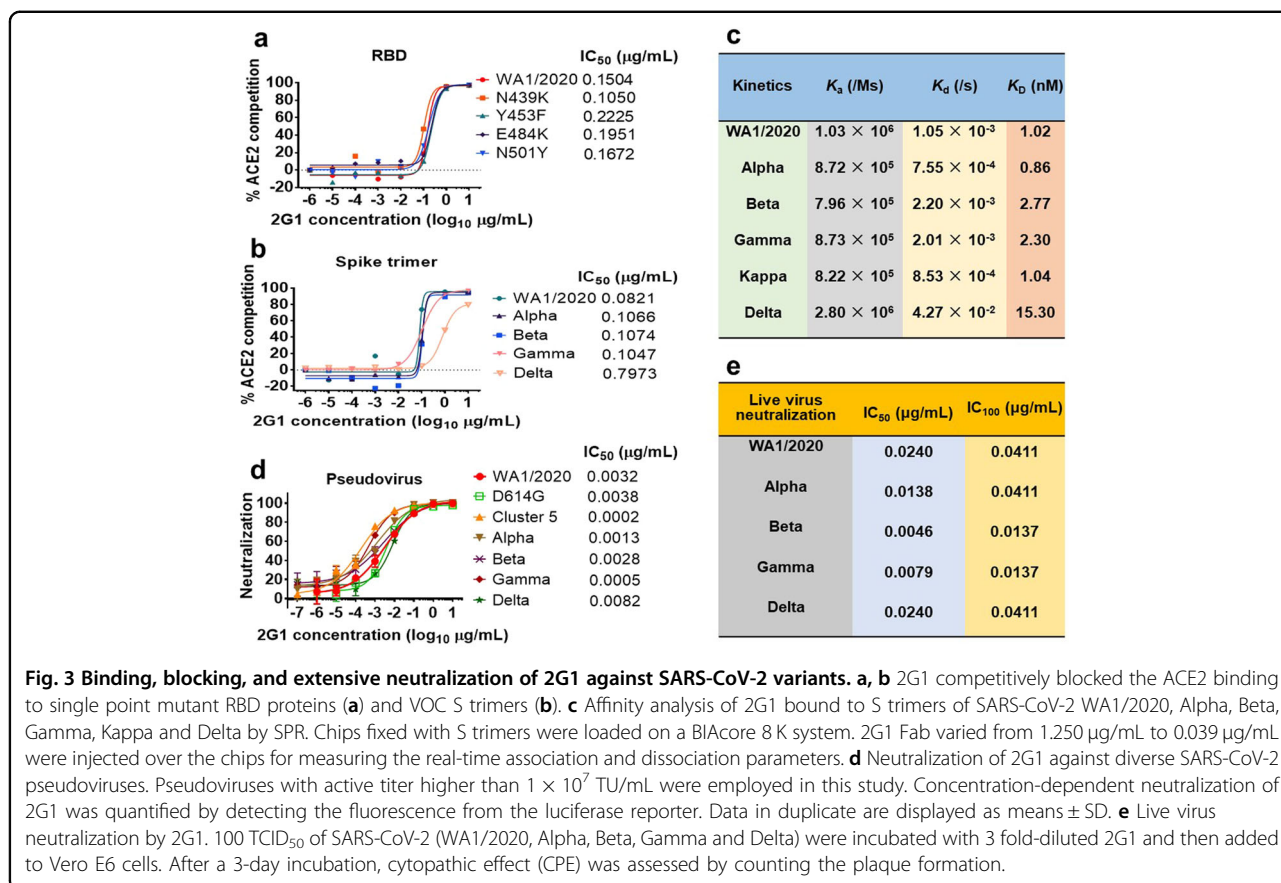


**Fig. 2 Characterization of 2G1 using WA1/2020 related S and RBD proteins and pseudovirus.** **a, b** 2G1 concentration-dependently binds to RBD-mFc (**a**) and S trimer (**b**) of SARS-CoV-2 in ELISA test. A neutralizing antibody 5B2 targeting SARS-CoV-2 RBD was used as control. Values from two replicates are shown as means ± SD. **c** Serial 10 fold-diluted 2G1 was incubated with SARS-CoV-2 WA1/2020 pseudovirus and used to infect 293T-ACE2 cells. After 48 h incubation, the infection was quantified using a fluorescence detection kit. **d** Binding kinetics of 2G1 to SARS-CoV-2 RBD in SPR. Serial dilutions of 2G1 Fab were flowed through a chip fixed with RBD recombinant protein. The kinetics data were fitted with results from different concentrations.



### 2G1 neutralizing SARS-CoV-2 variants

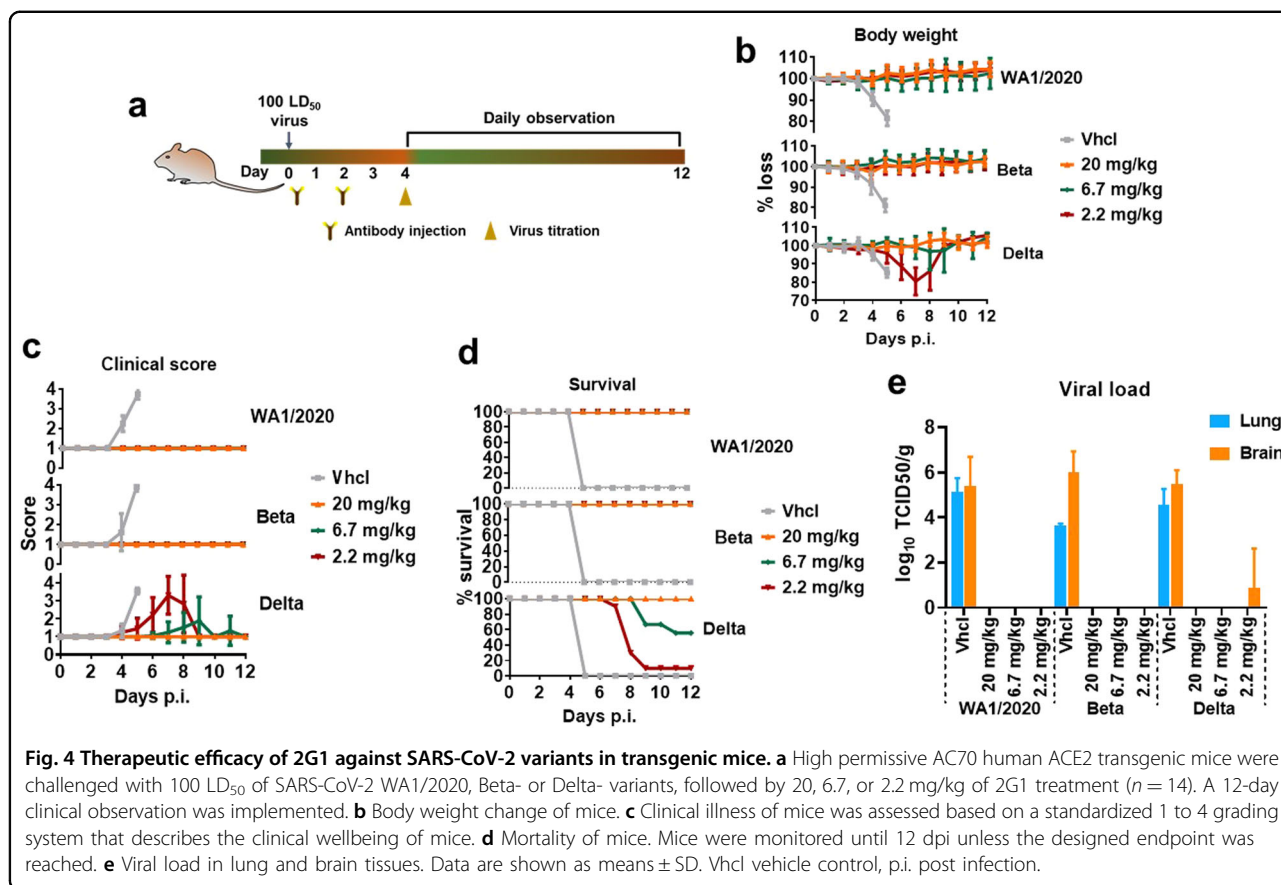
With the continuing spread of mutations, combating SARS-CoV-2 variants has become a crucial task. We explored the effects of 2G1 on the mutations at several important sites such as N439K, Y453F, E484K, and N501Y in terms of blocking the ACE2–RBD interaction. The  $IC_{50}$  of 2G1 blocking WA1/2020 RBD, N439K, Y453F, E484K and N501Y interacting with ACE2 were 0.1504, 0.1050, 0.2225, 0.1951 and 0.1672  $\mu\text{g/mL}$ , respectively (Fig. 3a). To further study the S mutants of VOCs influence on blocking ability of 2G1, mutant trimeric S proteins of VOCs were used in ACE2 blocking experiment. The  $IC_{50}$  of 2G1 were 0.0821, 0.1066, 0.1074, 0.1047, and 0.7973  $\mu\text{g/mL}$ , corresponding to WA1/2020, Alpha, Beta, Gamma, and Delta (Fig. 3b). We determined the affinities of 2G1 with various S trimers using SPR. 2G1 Fab bound to S trimers with nanomolar affinities.  $K_D$  of its binding to WA1/2020, Alpha, Beta, Gamma, Kappa, and Delta were 1.02, 0.86, 2.77, 2.30, 1.04, and 15.30 nM, respectively (Fig. 3c). The dissociation rate of 2G1/Delta ( $K_d = 4.27 \times 10^{-2}/\text{s}$ ) was increased as compared with WA1/2020 ( $K_d = 1.05 \times 10^{-3}/\text{s}$ ), which leads to the decrease in affinity.

In pseudovirus neutralization assays, we found that antibody 2G1 robustly neutralized all pseudoviruses,

including D614G, Alpha, Beta, Gamma, Delta, and Cluster 5 variants (Fig. 3d, Supplementary Fig. S3) with low  $IC_{50}$ , especially 0.0005  $\mu\text{g/mL}$  against Gamma and 0.0002  $\mu\text{g/mL}$  against Cluster 5. Live SARS-CoV-2 neutralization assay results were consistent with those from experiments using pseudoviruses. Antibody 2G1 neutralized WA1/2020 live virus with  $IC_{50}$  of 0.0240  $\mu\text{g/mL}$  (Fig. 3e) while it was more inclined to neutralize Alpha, Beta, and Gamma live virus, with  $IC_{50}$  decrease about 1.7-fold (0.0138  $\mu\text{g/mL}$ ), 5.2-fold (0.0046  $\mu\text{g/mL}$ ), and 3.0-fold (0.0079  $\mu\text{g/mL}$ ), respectively. In this assay, 2G1 had the same neutralizing activity ( $IC_{50} = 0.0240 \mu\text{g/mL}$ ) against Delta and WA1/2020.

### In vivo protection in animal models

To evaluate in vivo antiviral efficacy of 2G1 against SARS-CoV-2 challenge, we performed viral clearance assay employing both ACE2 transgenic mouse and rhesus macaque models. In the transgenic mouse study, animals were challenged with high copies of 100 times of half lethal dose ( $LD_{50}$ ) of SARS-CoV-2 WA1/2020, Beta, or Delta at day 0, followed by three different 2G1 dose treatments (20, 6.7 or 2.2 mg/kg) or vehicle injection with phosphate buffer saline (PBS). Four days post infection (dpi), four mice in each group including vehicle and



differentially treated groups were euthanized, and lungs and brains were collected for the titration of viral load (Fig. 4a). Mice treated with vehicle developed an acute wasting syndrome and quickly met the designed endpoint at 5 dpi. In contrast, WA1/2020 or Beta virus-infected mice that received 20, 6.7 or 2.2 mg/kg treatments survived without losing any weight or revealing any obvious signs of illness throughout the study (Fig. 4b–d). Delta virus-infected mice in the 20 mg/kg group all survived throughout the trial period and had a good clinical well-being score. In the same study, 55.6% mice in the 6.7 mg/kg group and 10% mice in the 2.2 mg/kg group recovered back to healthy physiological condition (Fig. 4b–d) from the virus challenge. Only a small amount of virus was detected in the brain tissue of the 2.2 mg/kg group of Delta-infected mice (Fig. 4e). The results indicated that at the range of 6.7–20 mg/kg, 2G1 antibody treatment was effective for animals to recover from the viral infection.

In the study of rhesus macaque model (Fig. 5a), the animals were infected with 10<sup>5</sup> half tissue culture infectious dose (TCID<sub>50</sub>) of SARS-CoV-2 (2019-nCoV-WIV04) per animal and randomly divided into control (vehicle injection), low-dose (10 mg/kg of 2G1), and high-dose (50 mg/kg of 2G1) groups, with one male and one female in each group. Drugs were intravenously given 24 h

post infection. All animals in the two therapy groups had a high viral load of 10<sup>6</sup> copies/mL in the throat swab at 1 dpi. After the drug injection, the viral titer gradually decreased. The throat virus was cleared at 3 dpi in one of the high-dose animals and at 4 dpi in the remaining treated animals (Fig. 5b). One animal in the control group had an elevated viral titer in the anal swab at 5 dpi, but no animals in the antibody-treated groups showed this trend until 7 dpi (Fig. 5c). In addition, we checked the viral distribution in lung, trachea, and bronchus tissues. The virus was detectable in most areas of the lungs, in the tracheas, and bronchi of the control animals. In the group treated with high-dose antibody, the virus was present in right-middle, left-middle, and left-lower of the lungs, as well as left-bronchi. In the low-dose group, the virus was only found in tracheas (Fig. 5d). Results from both transgenic mouse and rhesus macaque studies showed a promising protective efficacy of 2G1, in consistent with the in vitro neutralization results.

We further investigated the Fc effector function of 2G1. Results showed that 2G1 had no obvious antibody-dependent cellular cytotoxicity (ADCC) effect (not shown) but moderate antibody-dependent cellular phagocytosis (ADCP) up to 35% (Supplementary Fig. S4a). We hypothesize that the moderate ADCP may help the

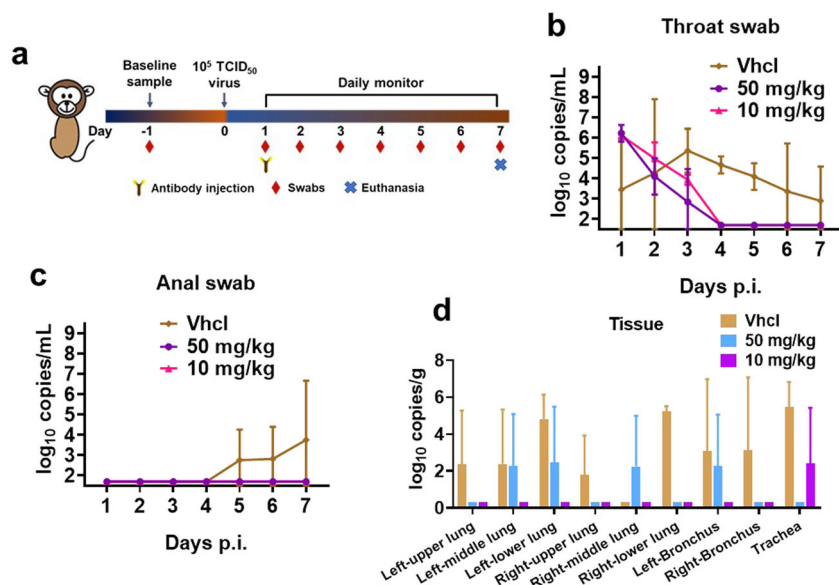


**Fig. 5** Therapeutic efficacy of 2G1 against SARS-CoV-2 variants in rhesus macaques. **a** One male and one female rhesus macaques in each group were endotracheally challenged with  $1 \times 10^5$  TCID<sub>50</sub> of SARS-CoV-2. 2G1 at 10 mg/kg or 50 mg/kg, or equal amount of PBS were intravenously given at 1 dpi. Throat and anal swabs were sampled daily until 7 dpi. **b** Viral load in throat swab. **c** Viral load in anal swab. **d** Viral load in lungs, tracheas, and bronchi. Data with duplications are shown as means  $\pm$  SD. Vhcl vehicle control, p.i. post infection.

antigen presentation of SARS-CoV-2. Pharmacokinetic study revealed that the half-life of 2G1 in mice was 11.1 days (Supplementary Fig. S4b), similar to many therapeutic antibodies. Mice treated with 15 mg/kg, 30 mg/kg, or 60 mg/kg showed no statistical changes in body weight, white blood cell count, red blood cell count, hemoglobin, and platelets (Supplementary Fig. S4c–g). Mice receiving 2G1 treatment had no obvious pathological changes in hearts, livers, spleens, lungs and kidneys (Supplementary Fig. S5). Currently, Investigational New Drug-directed systematic safety assessment is ongoing to support the pre-clinical safety of using 2G1 in human clinical trials. Toxicology study in non-human primate showed that 2G1 was well tolerated at the maximum experimented dosage of 200 mg/kg.

#### Cryo-EM structure of the complex between 2G1 and SARS-CoV-2 S protein

To investigate the binding mode of antibody 2G1 on S trimer, we solved the cryo-electron microscopy (cryo-EM) structure of 2G1 in complex with S trimer at 2.7 Å resolution (Fig. 6a; Supplementary Figs. S6 and S7). Yet, the cryo-EM map density on the interface between RBD and 2G1 was smeared. So, we performed local refinement and improved the antibody-antigen interface resolution to 3.2 Å, enabling reliable analysis of the interactions between the RBD and 2G1 (Fig. 6b). In the S/2G1 complex, three solved Fabs bound to trimeric S with all RBDs in the “down” position and the S protein in a locked conformation<sup>33,34</sup>

(Fig. 6a). There is an additional density in RBD domain of the structure, which was reported as free fatty acid linoleic acid (LA) in a locked conformation<sup>33</sup>.

For detailed analysis of the interface, antibody 2G1 binds to tip area of RBD of S trimer, overlapping with the ACE2 binding site on RBD and offset from the major mutational hotspots in VOCs. The heavy chain of 2G1 interacts with RBD mainly through three complementarity-determining regions (CDRs), named CDRH1 (residues 30–35), CDRH2 (residues 50–65), and CDRH3 (residues 98–111). The light chain of 2G1 participates interaction mainly through two CDRs, CDRL1 (residues 23 to 36) and CDRL3 (residues 91–100) (Fig. 6b–e). The interface between RBD and 2G1 is stabilized by an extensive hydrophobic interaction network. Phe486 on the RBD top loop interacts with Tyr33, Tyr52 on heavy chain and Tyr34, Tyr93, and Trp99 on light chain through hydrophobic and/or  $\pi$ - $\pi$  interactions simultaneously (Fig. 6c). CDRH1 and CDRH3 of the 2G1 heavy chain were positioned above the LA-binding pocket in the adjacent RBD' (Fig. 6b, e). We further compared 2G1 with three antibodies (S2E12, B1-182.1, and REGN10933), which have similar patterns of epitope (Fig. 7a–c). Structural comparison reveals that the epitope for 2G1 partially overlaps with these three antibodies (S2E12, B1-182.1, and REGN10933), but they have different binding directions (Fig. 7b and Supplementary Fig. S8). Neutralizing activity comparison shows as good activity of 2G1 as S2E12, B1-182.1, and REGN10933 (Fig. 7d). Besides, 2G1 has a relative narrow binding epitope which may result in lower

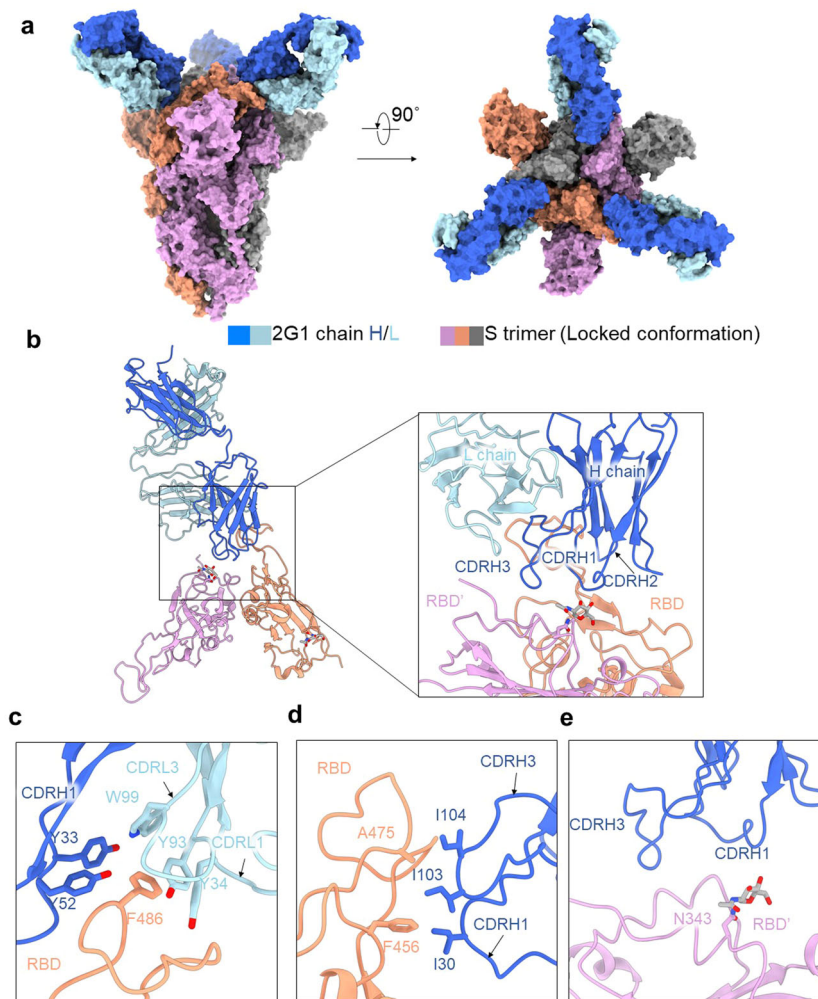


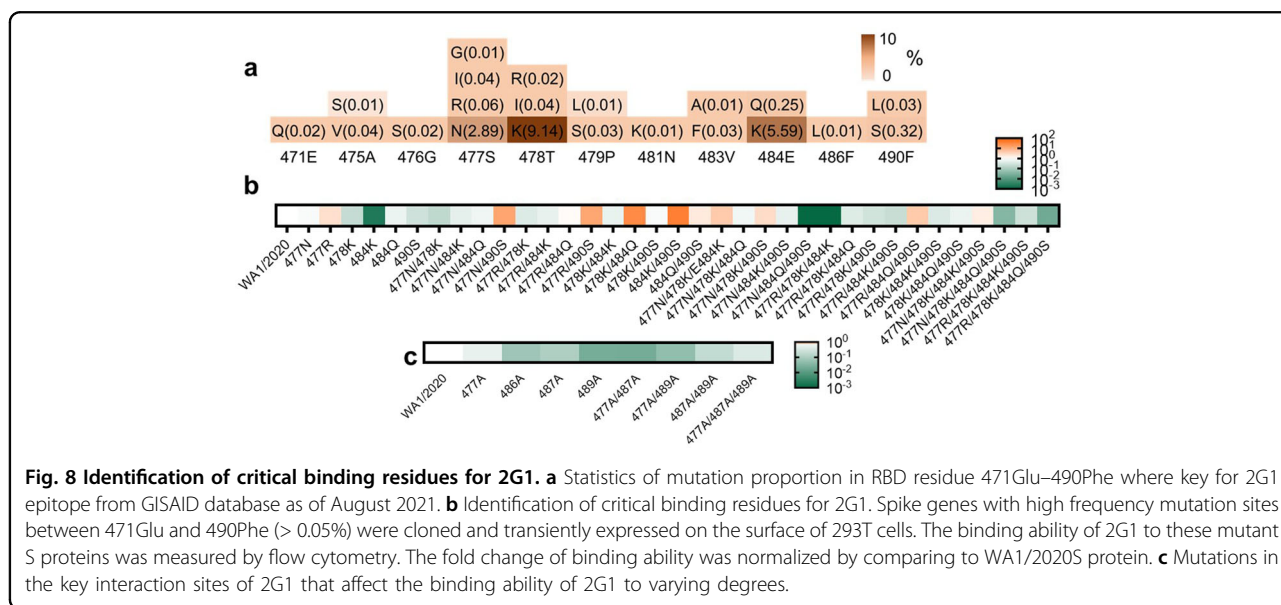
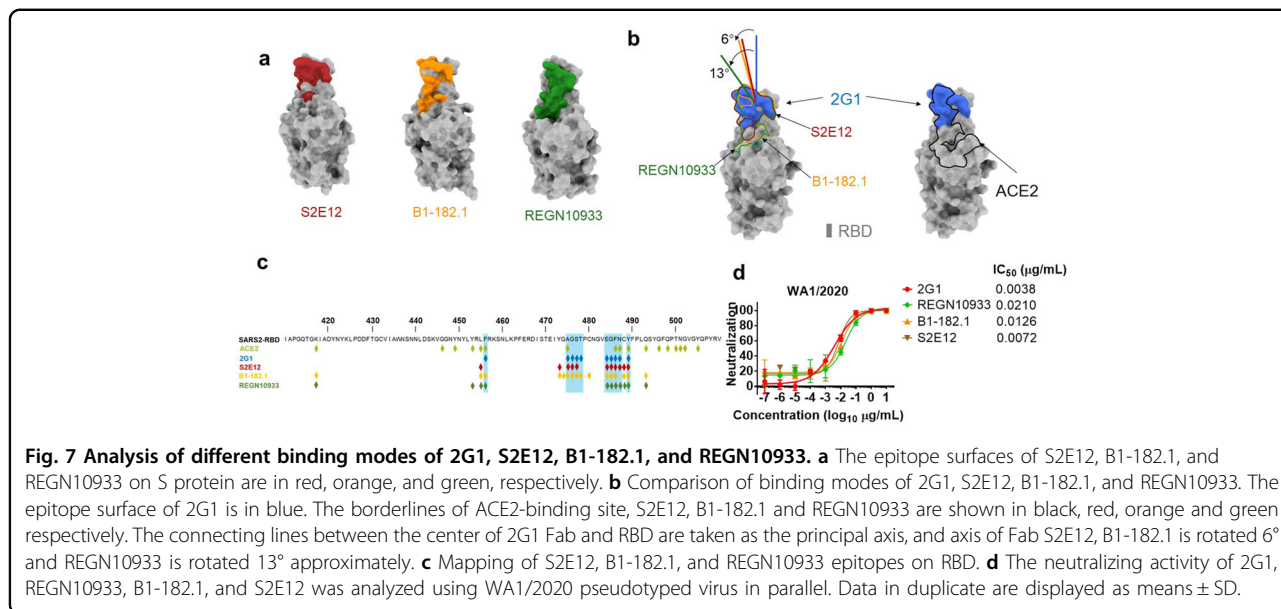
**Fig. 6** Cryo-EM structure of 2G1 and the complex with WA1/2020S protein. **a** The domain-colored cryo-EM map of SARS-CoV-2S ectodomain trimer and 2G1 Fab fragments complex is shown, viewed along two perpendicular orientations. The heavy and light chains of 2G1 are colored blue and cyan, respectively. The three protomers of trimeric S protein are colored gray, orange and pink. **b–e** The binding interface between 2G1 and RBD and adjacent RBD'. RBD and 2G1 interact with each other mainly through hydrophobic interactions (**c, d**). 2G1 heavy chains (CDRH3 and CDRH1) lie above the adjacent RBD' (**e**). Residues are numbered using the Kabat convention.

probability of losing neutralizing activity due to viral mutagenesis (Fig. 7c).

#### Potential escape risk evaluation

To address the potential virus escape issue, we collected the high-frequency mutation sites near the 2G1 binding epitope from GISAID database as of August 2021 (Fig. 8a), and constructed a series of S protein sequences containing these mutations. The change in binding ability of 2G1 was reflected by the normalized mean fluorescent intensity (MFI) relative to the WA1/2020S protein in flow cytometry. Mutants 484K, 477N/484Q/490S, and 477R/478K/484K distinctly reduced 2G1 binding (Fig. 8b). Mutants 477N/490S, 477R/490S, 478K/484Q, and 484K/490S remarkably enhanced 2G1 binding (Fig. 8b). The

484K substitution is featured in variants Beta and Gamma. Although 484K alone leads to a decreased binding ability of 2G1, trimeric S harboring all mutation sites only slightly influenced the affinity of 2G1 (Fig. 3c). The 484K substitution leads to the loss of salt bridge between Glu484 and ACE2 Lys31, resulting in the reduced affinity of ACE2<sup>35</sup>. It may be one of the reasons why the activity of 2G1 even slightly improved in neutralizing Beta and Gamma mutants. Another substitution in residue 484 with Gln (484Q) only slightly weakened the binding of 2G1 (Fig. 8b). SARS-CoV-2 Delta variant possesses the T478K substitution, which is a contact residue with 2G1. The single point mutation with T478K has mildly decreased the 2G1 binding (Fig. 8b), which is consistent with the SPR data.



We also directly mutated the key interacting residues between RBD and 2G1 by alanine substitution, though they are not high-frequency mutation sites. Only moderate decline in 2G1 interaction was found in several mutations, including 486A, 489A, 477A/487A, and 477A/489A (Fig. 8c). These results suggest that 2G1 could potentially be effective against future SARS-CoV-2 variants.

**Discussion**

SARS-CoV-2 has no sign of stopping its transmission since the outbreak, and the emergence of variants with increased transmissibility and capability of surveillance

escape has assisted its continued existence. Recently, the variant Delta has become an intensively concerned strain due to its unparalleled transmissibility, which is embodied in the 1000 times higher viral load than the ancestral strain of SARS-CoV-2<sup>6,36</sup>. The high-frequency mutation nature of SARS-CoV-2 necessitates the development of therapies with breadth<sup>37,38</sup>. We screened antibodies with broad spectrum of neutralizing effects from convalescent subjects. One of them, 2G1, showed excellent and extensive neutralization against both ancestral SARS-CoV-2 WA1/2020 and VOCs at sub-nanomolar IC<sub>50</sub> level. In the in vivo study, transgenic mice infected by the WA1/2020- or Beta- virus were cured by antibody 2G1 at a dose as low

as 2.2 mg/kg, as well as fully protected from Delta infection in the range from 6.7 to 20 mg/kg, even when animals were challenged with 100 times  $LD_{50}$  of viral load. These results indicate that 2G1 is a potent therapeutic antibody against a broad spectrum of current variants.

The cryo-EM structure of 2G1 in complex with the S protein revealed that 2G1 binds to the tip of S trimer through small interface but strong hydrophobic effect. The strong hydrophobic effect provides high affinity for 2G1, and the  $K_D$  of interaction with S trimers of SARS-CoV-2 and VOCs ranges from 0.86 to 15.3 nM. SARS-CoV-2 variants Beta and Gamma possess E484K and N501Y substitutions, which are adjacent to the epitope of 2G1. We correspondingly detected a slight decrease in the affinity of 2G1, from 1.02 nM for WA1/2020 to 2.77 nM for Beta and 2.30 nM for Gamma. Surprisingly, 2G1 showed no compromise in activity against Beta and Gamma in both pseudo-viruses and live-viruses, and both in vitro and in vivo. The dose of 2.2 mg/kg of 2G1 completely cleared the viral load in Beta virus-challenged transgenic mice, and the efficacy was as good as for WA1/2020 virus-challenged mice. The  $IC_{50}$  even improved in the in vitro live virus test, decreased from 0.0240  $\mu\text{g}/\text{mL}$  against WA1/2020 to 0.0046  $\mu\text{g}/\text{mL}$  against Beta and 0.0079  $\mu\text{g}/\text{mL}$  against Gamma. These results suggest that changes in affinity may not ultimately determine the therapeutic effect of neutralizing antibodies, and various other factors could be involved<sup>35,39</sup>. In addition, the small binding epitope reduces the probability of interference between 2G1 and other RBD antibodies so that 2G1 can cooperatively work with those antibodies to achieve a synergistic effect, for better responding to immunologic evasion of SARS-CoV-2 variants.

Furthermore, the specific 2G1 antibody epitope of RBD tip is offset from mutational hot spots and increases neutralization breadth covering new-onset VOCs. Variants Lambda comprising L452Q/F490S and Mu comprising E484K/N501Y in RBD have recently raised concerns<sup>28,29</sup>. Although residue 490 is close to 2G1 epitope, our results suggested that F490S did not cause significant affinity alteration. The E484K/N501Y substitution in variant Mu is also seen in Beta and Gamma. In view of the good binding and neutralization of 2G1 against Beta and Gamma, we believe that 2G1 will likely be comparatively effective against Mu. In addition, we directly mutated the amino acid residues adjacent to the epitope on RBD by 2G1, as well as several residues that directly interact with 2G1, and found that only few mutation groups may cause a significant weakening of the 2G1 binding ability. Collectively, the model of 2G1 binding to the tip of S trimer provides a good reference for developing vaccines and optimizing a better combination therapy.

The neutralizing antibody 2G1 has been manufactured under cGMP to support the Investigational New Drug

application. We would believe that antibody treatment with 2G1 will bring clinical benefit to COVID-19 patients.

## Materials and methods

### B cells

Blood samples were obtained from patients who were recovered from COVID-19 for 10 weeks and had a negative nucleic acid test. Samples with serum antibody titer over  $1 \times 10^6$  were chosen for the PBMC separation using Ficoll density gradient centrifugation method. B cells were enriched with a human B Cell Isolation Kit (Stemcell). Afterwards, B cells were then stained with APC-Alex700 labeled anti-CD19 (BD), BV421 labeled anti-CD27 (BD), BV510 labeled anti-IgG (BD), Biotin labeled RBD (Sino Biological), PE labeled streptavidin (ThermoFisher) and 7AAD (BD). Single memory B cells with potential SARS-CoV-2 antibody secretion were sorted out by gating 7AAD<sup>-</sup>, CD19<sup>+</sup>, CD27<sup>+</sup>, IgG<sup>+</sup>, and RBD<sup>+</sup> using a BD Aria III cell sorter with fluorescence-activated cell sorting modules. B cells were suspended into lysis buffer and quickly frozen. B cell mRNA was subsequently converted to cDNA by SuperScript III Reverse Transcriptase (Invitrogen) and V genes were rescued by PCR. Linear Cassettes were composed of CMV promoter  $V_H$  or  $V_L$  and polyA tail, and were used for expressing a small amount of antibody for preliminary screening.

### mAb preparation

Genes encoding heavy chains and light chain were inserted separately into pcDNA3.4 and amplified in *E. coli* DH5 $\alpha$ . PureLink™ HiPure Plasmid Miniprep Kit (Invitrogen) was used for low endotoxin plasmid preparation. Monoclonal antibodies were transiently expressed by co-transfecting ExpiCHO-S cells (ThermoFisher) with heavy chain and light chain plasmids using an ExpiCHO™ Expression System (Gibco). Cell culture was harvested after an 8–14 day of incubation at 37 °C with humidified atmosphere of 8% CO<sub>2</sub> with shaking. Full-length IgG was obtained by affinity purification utilizing a Protein A chromatography column (GE Healthcare) in AKTA avant (Cytiva). For long-term storage, antibodies were kept in a solution containing 10 mM Histidine-HCl, 9% trehalose, and 0.01% polysorbate 80.

### 293T-ACE2 cells

To obtain HEK-293T cells with stable expression of ACE2 protein, a lentiviral system bearing ACE2 (Genbank ID: BAJ21180.1) gene was constructed. In brief, HEK-293T cells (ATCC) with 70%–80% confluence in a 10 cm dish were co-transfected with 12  $\mu\text{g}$  of plasmid pHIV-puro encoding RRE and ACE2 genes, 8  $\mu\text{g}$  of plasmid psPAX2 encoding gag and pol, and 4  $\mu\text{g}$  of plasmid VSV-G encoding G glycoprotein of vesicular stomatitis virus(VSVG) using Lipofectamine 3000 Reagent (Invitrogen). Twelve hours

later, the medium was changed to fresh DMEM (Gibco) supplemented with 10% fetal bovine serum (Gibco) for another 48 h culturing. Medium containing virus particles was harvested and concentrated using a Lentivirus Concentration Kit (Genomeditech). The concentrated virus particles were used to infect HEK-293T cells under selection pressure of 10  $\mu\text{g}/\text{mL}$  puromycin (Beyotime Biotechnology). The transfection efficiency was examined by flow cytometry using S1-mFc recombinant protein (Sino Biological) as primary antibody and FITC-AffiniPure Goat Anti-Mouse IgG (Jackson) as secondary antibody. The resulting bulk transfected population was sorted on a BD FACSJazz Cell Sorter (BD) with the BD FACS™ Software. Cells with top 1% fluorescence intensity were retained and expanded for subsequent use.

### S protein overexpression cells

The coding sequence for full-length WA1/2020 S protein (GenBank: QHD43416.1) from Met1 to Thr1273 was inserted into plasmid pHIV-puro1.0, followed by an internal ribosome entry site and puromycin resistance gene. The lentiviruses were generated using the HEK-293T packaging system as mentioned above. Five hundred microliter of filtered lentivirus supernatant was added in a 24-well plate with Jurkat cells (ATCC). After cell expansion and selection with 10  $\mu\text{g}/\text{mL}$  puromycin for 1 week, the positive S expression was confirmed by flow cytometry.

### Antigen-binding ELISA

ELISA was applied to study the binding ability of antibodies with SARS-CoV-2 RBDs (Sino Biological) and S trimers (AcroBiosystems). Antigens were diluted with ELISA Coating Buffer (Solarbio) to 1.0  $\mu\text{g}/\text{mL}$  and immobilized onto High Binding ELISA 96-Well Plate (BEAVER) with 100  $\mu\text{L}$  per well overnight at 4 °C. Plates were washed four times with PBST (Solarbio) and blocked with 3% skim milk for 1 h at 37 °C. Then, serially diluted antibodies were added 100  $\mu\text{L}$  per well and incubated at 37 °C for 1 h. After pipetting off the unbound antibodies, plates were washed four times with PBST and further incubated with 100  $\mu\text{L}$  per well of goat anti-human IgG (Fc specific)-Peroxidase antibody (1:5000 dilution, Sigma) for 1 h at 37 °C. After a final four times washing with PBST, the binding of antibodies with SARS-CoV-2 antigens were visualized by adding 100  $\mu\text{L}$  peroxidase substrate TMB Single-Component Substrate solution (Solarbio) and incubating for 15 min in dark. The reaction was terminated by adding 50  $\mu\text{L}$  stop buffer (Solarbio) and the plates were immediately submitted to an ELISA microplate reader (TECAN Infinite M200 Pro) to measure the optical density (OD) at 450 nm. Data were analyzed with GraphPad Prism Version 9.0.0 and  $EC_{50}$  values were determined using a four-parameter nonlinear regression.

### ACE2 competition ELISA

For experiments involving the competitive binding of antibodies to SARS-CoV-2 RBD or S trimer, recombinant hACE2-Fc protein was first biotinylated using EZ-Link Sulfo-NHS-Biotin (ThermoFisher) as the instruction described. SARS-CoV-2 RBD (Sino Biological), S trimer (AcroBiosystems), mutated RBDs (Sino Biological), and mutated S trimers (AcroBiosystems) were coated onto High Binding ELISA 96-Well Plate (BEAVER). In order to obtain an optimized hACE2-Fc concentration for this experiment, the concentration-dependent binding of biotinylated hACE2-Fc to coated SARS-CoV-2 antigens was measured by performing a conventional receptor-binding ELISA. The 80% maximal effective concentration ( $EC_{80}$ ) of biotinylated hACE2-Fc was calculated by the four-parameter nonlinear fitting. Antibodies were serially diluted in 1% BSA (Sigma) and added 50  $\mu\text{L}$  into the antigen coated plates. Biotinylated hACE2-Fc at  $EC_{80}$  concentration was subsequently pipetted into. After incubation at 37 °C for 1 h, plates were washed four times with PBST and incubated with 100  $\mu\text{L}$  of 1:2000 diluted Ultrasensitive Streptavidin-Peroxidase Polymer (Sigma). After further washing, 100  $\mu\text{L}$  TMB was added, followed by detection of the bound hACE2 in the microplate reader. Four-parameter nonlinear regression fitting in GraphPad Prism Version 9.0.0 was applied for result analysis.

### SPR

The binding affinities of antibodies to SARS-CoV-2 RBD and S trimers (WA1/2020/B.1.1.7/B.1.351/P.1/B.1.617.1/B.1.617.2) were tested using a BIAcore 8K system (Cytiva) together with CM5 biosensor chips (Cytiva). Antigens were diluted in pH 5.0 Acetate (Cytiva) and covalently coupled on chips using an Amine Coupling Kit (Cytiva). After reaching a 70 RU coupling level, the excess antigens were washed away and the unbound sites were blocked with ethanolamine. Antibodies were 2-fold serially diluted from 1.250 to 0.039  $\mu\text{g}/\text{mL}$  in HBS-EP buffer (Cytiva) and then injected for 120 s at 30  $\mu\text{L}/\text{min}$ . After that, the binding was dissociated with HBS-EP buffer for 120 s, followed by chip regeneration with pH 1.5 Glycine (Cytiva). Parameters including  $K_a$ ,  $K_d$ , and  $K_D$  values were calculated employing a monovalent analyte model with BIAevaluation software.

### Pseudovirus neutralization

ACE2-293T cells were seeded in a white 96-well plate (Corning) at a density of  $1 \times 10^4$  cells per well one night prior to use. Serially diluted antibodies were incubated with WA1/2020 (Yeasen) or mutant pseudoviruses (GENEWIZ) for 0.5 h at 37 °C. Human ACE2-Fc or other SARS-CoV-2 RBD-specific antibodies were used as a positive control to validate data collection in different panels of screening. Medium containing equal amount of

pseudoviruses but no antibodies was used as blank control. The culture medium of ACE2-293T cells was removed and then replaced by the antibody-pseudovirus mixture. All operations were conducted in the BSL-2 lab in Shanghai Jiao Tong University. After an additional 48 h of incubation, the luminescence of each well was measured using a ONE-Glo™ Luciferase Assay System (Promega) in the Infinite M200 Pro NanoQuant (TECAN). The acquired luminescence units were normalized to those of blank control wells. Dose-dependent neutralization curves were fitted using a four-parameter nonlinear regression in GraphPad Prism Version 9.0.0.

### Plaque reduction neutralization

Plaque reduction neutralization test was performed using SARS-CoV-2 WA1/2020 (US\_WA-1/2020 isolate), Alpha (B.1.1.7/UK, Strain: SARS-CoV-2/human/USA/CA\_CDC\_5574/2020), Beta (B.1.351/SA, Strain: hCoV-19/USA/MD-HP01542/2021), Gamma (P.1/Brazil, Strain: SARS-CoV-2/human/USA/MD-MDH-0841/2021), and Delta variants (B.1.617.2/Indian, Strain: GNL-751, a recently isolated strain from Galveston County, Texas) at Galveston National Laboratory at University of Texas Medical Branch at Galveston, Texas. Briefly, antibodies were 3-fold serially diluted in MEM medium (Gibco) from 20 µg/mL for preparing the working solution. The dilutions were mixed with equal volume of 100 TCID<sub>50</sub> virus in two replicates and incubated at room temperature for 1 h. The mixture was then added into a 96-well plate covered with Vero cells. Blank controls and virus infection controls were set up simultaneously. After incubation at 37 °C, 5% CO<sub>2</sub> for 3 days, cytopathic effect (CPE) was observed under microscope and plaques were counted for efficacy evaluation. Wells with CPE changes are recorded as “+”, otherwise recorded as “-”. IC<sub>50</sub> values were calculated according to the following equation:  $IC_{50} = \text{Antilog} \left( \frac{D - C \times (50 - B)}{A - B} \right)$ , where *A* indicates the percentage of inhibition higher than 50%, *B* indicates the percentage of inhibition less than 50%, *C* is log<sub>10</sub> (dilution factor), *D* is log<sub>10</sub> (sample concentration) when the inhibition is less than 50%.

### ACE2 transgenic mouse protection

AC70 human ACE2-transgenic mice (Taconic Biosciences) were divided into control (100 µL PBS) and treatment (20, 6.7, or 2.2 mg/kg of 2G1, 100 µL) groups, with 14 mice in each group. Animal studies were carried out at Galveston National Laboratory at University of Texas Medical Branch at Galveston, Texas, an AAALAC accredited (November 24, 2020) and PHS OLAW approved (February 26, 2021) high-containment National Laboratory, based on a protocol approved by the Institutional Animal Care and Use Committee at UTMB at Galveston. Mice were challenged with 100 LD<sub>50</sub> of SARS-

CoV-2 (US\_WA-1/2020 isolate), Beta (B.1.351/SA, Strain: hCoV-19/USA/MD-HP01542/2021), or Delta variant (B.1.617.2/Indian, Strain: GNL-751, a recently isolated strain from Galveston County, Texas), provided through World Reference Center for Emerging Viruses and Arboviruses (WRCEVA) were used in the study. The first dose of antibody 2G1 and PBS were given 4 h of post-infection; and the second was given 2 days of post-infection. Mice were clinically observed at least once daily and scored based on a 1–4 grading system that describes the clinical wellbeing. In the standardized 1–4 grading system, score 1 is healthy; score 2 is with ruffled fur and lethargic; score 3 is with additional clinical sign such as hunched posture, orbital tightening, increased respiratory rate, and/or > 15% weight loss; score 4 is showing dyspnea and/or cyanosis, reluctance to move when stimulated, or ≥ 20% weight loss that need immediate euthanasia. Four mice in each group were euthanized at 4 dpi for assessing viral loads and histopathology of lung and brain. The remaining ten mice were continue monitored for morbidity and mortality for up to 12 dpi.

### Rhesus macaque protection

Rhesus macaques at 6–7 years old were purchased from Hubei Tianqin Biotechnology Co., Ltd. All animal procedures and operations were approved by the ethical committee of Wuhan Institute of Virology, Chinese Academy of Sciences. SARS-CoV-2 strain 2019-nCoV-WIV04 (GISAID number: EPI\_ISI\_402124) was isolated from the bronchoalveolar lavage fluid of a patient who was infected COVID-19 in Wuhan in December 2019. Rhesus macaques were randomly divided into control group, low-dose (10 mg/kg of 2G1) and high-dose (50 mg/kg of 2G1) groups with one male and one female in each. Animals were endotracheally infected with 4 mL of  $1 \times 10^5$  TCID<sub>50</sub> virus. Antibody 2G1 and PBS were intravenously given 24 h after infection. Rhesus macaques were monitored for disease-related changes during the period. Body weight and temperature were measured every day, and throat swab and anal swab samples were collected for virus titrating. Animals were euthanized at 7 dpi and tissue samples were collected for virus examining. Viral RNA was extracted using the QIAamp Viral RNA Mini Kit (Qiagen). A one-step real-time quantitative PCR was used to quantify the viral RNA according to the supplier's instructions (HiScript® II One Step qRT-PCR SYBR® Green Kit, Vazyme Biotech Co., Ltd) together with primers for the RBD gene (RBD-qF1: 5'-CAA TGGTTAAGGCAGG-3'; RBD-qR1: 5'-CTCAAGGTCTG GATCACG-3').

### ADCP

In ADCP experiment, CD14<sup>+</sup> monocytes (Allcells) were cultured and differentiated for 7 days to obtain macrophage cells. Macrophages were labeled with violet dye

(ThermoFisher), and Jurkat cells with stable SARS-CoV-2 S expression were labeled with CFSE dye (ThermoFisher). 75,000 Jurkat cells were added to macrophage cells in a 96-well plate in the presence of 2G1 or the isotype control antibody. After incubating at 37 °C for 30 min, the macrophages were digested and fixed with 4% paraformaldehyde, and the proportion of double-positive cell populations was analyzed by flow cytometry.

#### Pharmacokinetic study and toxicity test

For the pharmacokinetic study, BALB/c mice were tail intravenously injected with 2G1 (15, 30, or 60 mg/kg), or equivalent volume of PBS. Three males and three females were in each subset. Blood samples were collected at 0.5, 6 h, 1, 2, 4, 7, 10, 15, 21, and 28 days after injection. Serum 2G1 concentration was quantified using ELISA. Briefly, mouse anti-human IgG Lambda (SouthBiotech) at 2 µg/mL was coated in ELISA plates. Serum samples and antibody 2G1 control were added into the plates and incubated for 1 h. After washing, a goat anti-human Fc HRP (Sigma) was used as secondary antibody with 1:6000 dilutions. After the chromogenic reaction by the HRP substrate (Solarbio), the plates were read at 450 nm.

Crj:CD1(ICR) mice were randomly divided into control (treated with PBS), 15, 30, and 60 mg/kg groups for testing the *in vivo* toxicity of 2G1, with three males and three females each group. Body weight was tracked every 2 days. Blood samples were collected 14 days after administration and mice were subsequently euthanized for tissue damage detection. Blood indicators including white blood cell count, red blood cell count, hemoglobin, and platelets were measured in multiple automated hematology analyzer (Sysmex XT-2000iV). Pathological changes of hearts, livers, spleens, lungs and kidneys were examined by hematoxylin and eosin (H&E) staining.

#### Expression and purification of S protein

The prefusion S extracellular domain (1–1208 aa) (Genbank ID: QHD43416.1) was cloned into the pCAG vector (Invitrogen) with six proline substitutions at residues 817, 892, 899, 942, 986, and 987<sup>39</sup>, a “GSAS” substitution (instead of “RRAR”) at residues 682–685 and a C-terminal T4 fibrin trimerization motif followed by one Flag tag.

Recombinant S protein was overexpressed using the HEK 293F mammalian cells (Invitrogen) at 37 °C under 5% CO<sub>2</sub> in a Multitron-Pro shaker (Infors, 130 rpm). For secreted S protein production, about 1.5 mg of the plasmid was premixed with 3 mg of polyethylenimines (PEIs) (Polysciences) in 50 mL of fresh medium for 15 min before added to cell culture, and transiently transfected into the cells, when the cell density reached  $2.0 \times 10^6$  cells/mL. Cells were removed by centrifugation at 4000× *g* for 15 min and cell culture supernatant was collected 60 h after transfection. The secreted S proteins were purified by anti-FLAG M2 affinity

resin (Sigma Aldrich). After loading two times, the anti-FLAG M2 resin was washed with the wash buffer containing 25 mM Tris (pH 8.0), 150 mM NaCl. The protein was eluted with the wash buffer plus 0.2 mg/mL flag peptide. The eluent was then concentrated and subjected to gel filtration chromatography (Superose 6 Increase 10/300 GL, GE Healthcare) in buffer containing 25 mM Tris (pH 8.0), 150 mM NaCl. The peak fractions were collected and concentrated to incubate with mAb. The purified S protein was mixed with the 2G1 at a molar ratio of about 1:5 for 1 h, respectively. Then the mixture was subjected to gel filtration chromatography (Superose 6 Increase 10/300 GL, GE Healthcare) in buffer containing 25 mM Tris (pH 8.0), 150 mM NaCl. The peak fractions were collected for EM analysis.

#### Cryo-EM sample preparation, data collection, and data processing

The peak fractions of complex were concentrated to about 2.5 mg/mL and applied to the grids. Aliquots (3.3 µL) of the S/2G1 complex were placed on glow-discharged holey carbon grids (Quantifoil Au R1.2/1.3). The grids were blotted for 2.5 or 3.0 s and flash-frozen in liquid ethane cooled by liquid nitrogen with Vitrobot (Mark IV, ThermoFisher). The prepared grids were transferred to a Titan Krios operating at 300 kV equipped with Gatan K3 detector and GIF Quantum energy filter. Movie stacks were automatically collected using AutoEMation<sup>40</sup>, with a slit width of 20 eV on the energy filter and a defocus range from  $-1.2$  to  $-2.2$  µm in super-resolution mode at a nominal magnification of 81,000×. Each stack was exposed for 2.56 s with an exposure time of 0.08 s per frame, resulting in a total of 32 frames per stack. The total dose rate was approximately  $50 \text{ e}^-/\text{Å}^2$  for each stack. The stacks were motion corrected with MotionCor2<sup>41</sup> and binned 2-fold, resulting in a pixel size of 1.087 Å/pixel. Meanwhile, dose weighting was performed<sup>42</sup>. The defocus values were estimated with Gctf<sup>43</sup>.

Particles for S in complex with 2G1 were automatically picked using Relion 3.0.6<sup>44–47</sup> from manually selected micrographs. After 2D classification with Relion, good particles were selected and subject to two cycles of heterogeneous refinement without symmetry using cryoSPARC<sup>48</sup>. The good particles were selected and subjected to Non-uniform Refinement (beta) with C1 symmetry, resulting in the 3D reconstruction for the whole structures, which was further subject to 3D auto-refinement and post-processing with Relion. For interface between S protein of SARS-CoV-2 and 2G1, the dataset was subject to focused refinement with adapted mask on each RBD-2G1 sub-complex to improve the map quality. The datasets of similar RBD-2G1 sub-complexes were combined if possible and necessary. The re-extracted dataset was 3D classified with Relion focused on RBD-2G1 sub-complex.

Then the good particles were selected and subject to focused refinement with Relion, resulting in the 3D reconstruction of better quality on RBD-2G1 sub-complex. The resolution was estimated with the gold-standard Fourier shell correlation 0.143 criterion<sup>49</sup> with high-resolution noise substitution<sup>50</sup>. Refer to Supplementary Figs. S6 and S7 and Table S1 for details of data collection and processing.

For model building of the complex of S of SARS-CoV-2 with 2G1, the atomic model of the S in complex 4A8 (PDB ID: 7C2L) was used as templates, which were molecular dynamics flexible fitted<sup>51</sup> into the whole cryo-EM map of the complex and the focused-refined cryo-EM map of the RBD-2G1 sub-complex, respectively. A Chainsaw<sup>52</sup> model of the 2G1 was first obtained using the 4A8 as a template, which was further manually adjusted based on the focused-refined cryo-EM map of the RBD-2G1 sub-complex with Coot<sup>53</sup>. Each residue was manually checked with the chemical properties taken into consideration during model building. Several segments, whose corresponding densities were invisible, were not modeled. Structural refinement was performed in Phenix<sup>54</sup> with secondary structure and geometry restraints to prevent overfitting. To monitor the potential overfitting, the model was refined against one of the two independent half maps from the gold-standard 3D refinement approach. Then, the refined model was tested against the other map. Statistics associated with data collection, 3D reconstruction and model building were summarized in Supplemental Table S1.

### Binding to S mutants on cell surface

Plasmids encoding full-length SARS-CoV-2 S (GenBank ID: QHD43416.1) with one or more mutation sites were carried into HEK-293T cells using lipofectamine 3000 (ThermoFisher) according to the manufacturer's instruction. After 48 h, cells were disassociated from the plates using a Cell Dissociation Buffer (ThermoFisher) followed by washing with PBS. Antibody 2G1 at 10 µg/mL was added into cells for 30 min incubation. Subsequently, cells were washed and incubated with Alexa Fluor 647 labeled Goat anti-Human IgG (ThermoFisher) for 30 min. After final washing, signals were acquired in flow cytometer (BD) and the binding ability to S mutants were evaluated by MFI.

### Acknowledgements

The authors would like to acknowledge following organizations and individuals for their assistances in the preparation of the manuscript: Professors Chuan Qin and Jiangning Liu from Institute of Laboratory Animal Sciences, CAMS & PUMC, China for their support in initial cell-based assay on neutralizing activity of the antibody generated in our lab; Dr. Liang Zhang of Jeicho Biopharmaceuticals Co., Ltd. for his input on potential clinical applications of the antibodies; Professor Buyong Ma of SJTU for discussion and analysis on the structural interaction between the virus and antibody; We thank the cryo EM facility and the High-Performance Computing Center of Westlake University for

providing supports. This work was funded by the National Natural Science Foundation of China (81773621, 82073751 to J.Z. 32022037, 31971123, 31800139 to Q.Z.); the National Science and Technology Major Project "Key New Drug Creation and Manufacturing Program" of China (2019ZX09732001-019 to J.Z.); the Key R&D Supporting Program (Special support for developing medicine for infectious diseases) from the Administration of Chinese and Singapore Tianjin Eco-city to Jeicho Biopharmaceuticals Ltd. Co.; Zhejiang University special COVID-19 grant 2020XGX099 and Shanghai Jiao Tong University "Crossing Medical and Engineering" grant 20X190020003 to J.Z. This work was funded by the Leading Innovative and Entrepreneur Team Introduction Program of Hangzhou, and Special Research Program of Novel Coronavirus Pneumonia of Westlake University and Tencent Foundation. We would like to express our sincere gratitude towards the generous supports from Tencent Foundation and Westlake Education Foundation.

### Author details

<sup>1</sup>Engineering Research Center of Cell and Therapeutic Antibody, Ministry of Education, China; School of Pharmacy, Shanghai Jiao Tong University, Shanghai, China. <sup>2</sup>Center for Infectious Disease Research, Westlake Laboratory of Life Sciences and Biomedicine, Key Laboratory of Structural Biology of Zhejiang, School of Life Sciences, Westlake University, Hangzhou, Zhejiang, China. <sup>3</sup>Institute of Biology, Westlake Institute for Advanced Study, Hangzhou, Zhejiang, China. <sup>4</sup>University of Texas, Medical Branch, Departments of Microbiology and Immunology, Galveston, TX, USA. <sup>5</sup>University of Texas, Medical Branch, Neurosciences, Cell Biology, and Anatomy, Galveston, TX, USA. <sup>6</sup>University of Texas, Medical Branch, Pathology, Galveston, TX, USA. <sup>7</sup>University of Texas, Medical Branch, Center for Biodefense and Emerging Disease, Galveston, TX, USA. <sup>8</sup>Jeicho Biopharmaceuticals Co., Ltd., Tianjin, China. <sup>9</sup>Jeicho Laboratories, Inc., Frederick, MD, USA. <sup>10</sup>National Institute for Viral Disease Control and Prevention, China CDC, Beijing, China. <sup>11</sup>Zhengzhou University People's Hospital; Henan Provincial People's Hospital, Department of Respiratory and Critical Care Medicine, Zhengzhou, Henan, China. <sup>12</sup>Zhengzhou University People's Hospital; Henan Provincial People's Hospital, Clinical Research Service Center, Zhengzhou, Henan, China. <sup>13</sup>Jeicho Institute, Co., Ltd., Shanghai, China

### Author contributions

L.H. and H.M. designed and conducted experiments on antibody binding activities, antibody neutralizing experiments using pseudovirus system and drafted the manuscript. L.H., H.T., H.Z., L.W., Y.K., Y.Y., H.Y., H.C., J.Zhang, and Y.L. conducted experiments on molecular discovery from blood sample to antibodies and characterization. M.W., J.L. and Y.Y. designed and executed animal study on metabolic profile and toxicology. C.-T.K.T., A.D., K.R.K. and B.-H. P. designed and executed in vitro and in vivo study on virus neutralizing activity. X.X. provided technical instructions on antibody screening from B cells. J.G. provided critical discussions and manuscript editing. Y.X. and H.J. coordinated project on molecular discovery, characterization, preparation, and provided critical discussions on in vitro and in vivo animal study on virus neutralization. X.Z., Z.W., L.Y. and Y.C. coordinated blood sample collection from convalescent individuals and facilitated B-cell screening. Z.W., Y.H., Y.C., G. Li, G.Liu, J.S., L.M. and Z.S.X. conducted sample preparation, quality control, and product characterization. Q.Z. conceived the project on structure analysis. Y.G. designed and did the cryo-EM experiments. Y.Z. solved the cryo-EM structures and Y.G. and Y.Z. analyzed the cryo-EM structures and prepared figures. S.W., H. H., A.W., K.Y., Z.S., H.C. and L.Z. conducted experiments on antibody expression, analytical development, and characterization. W.X., S.Z. and T.J., conducted in vitro virus neutralizing assays. Y.B. and B.Z. coordinated project activities and provided critical discussion. J.Zhu designed the overall project, organized and coordinated activities from all participating institutes, and revised manuscript.

### Competing interests

The authors declare no competing interests.

### Publisher's note

Springer Nature remains neutral with regard to jurisdictional claims in published maps and institutional affiliations.

**Supplementary information** The online version contains supplementary material available at <https://doi.org/10.1038/s41421-022-00381-7>.

Received: 27 October 2021 Accepted: 24 January 2022

Published online: 15 February 2022

## References

- Volz, E. et al. Assessing transmissibility of SARS-CoV-2 lineage B.1.1.7 in England. *Nature* **593**, 266–269 (2021).
- Alpert, T. et al. Early introductions and transmission of SARS-CoV-2 variant B.1.1.7 in the United States. *Cell* **184**, 2595–2604 (2021).
- Liu, J. et al. BNT162b2-elicited neutralization of B.1.617 and other SARS-CoV-2 variants. *Nature* **596**, 273–275 (2021).
- Dejnirattisai, W. et al. Antibody evasion by the P.1 strain of SARS-CoV-2. *Cell* **184**, 2939–2954 (2021).
- Chen, R. E. et al. In vivo monoclonal antibody efficacy against SARS-CoV-2 variant strains. *Nature* **596**, 103–108 (2021).
- Li, B. et al. Viral infection and transmission in a large, well-traced outbreak caused by the SARS-CoV-2 Delta variant. *Nat. Commun.* **13**, 460 (2022).
- Andreano, E. & Rappuoli, R. SARS-CoV-2 escaped natural immunity, raising questions about vaccines and therapies. *Nat. Med.* **27**, 759–761 (2021).
- Cohen, A. A. et al. Mosaic nanoparticles elicit cross-reactive immune responses to zoonotic coronaviruses in mice. *Science* **371**, 735–741 (2021).
- Ju, B. et al. Human neutralizing antibodies elicited by SARS-CoV-2 infection. *Nature* **584**, 115–119 (2020).
- Lv, Z. et al. Structural basis for neutralization of SARS-CoV-2 and SARS-CoV by a potent therapeutic antibody. *Science* **369**, 1505–1509 (2020).
- Chi, X. et al. A neutralizing human antibody binds to the N-terminal domain of the Spike protein of SARS-CoV-2. *Science* **369**, 650–655 (2020).
- Liu, Z. M. et al. Identification of SARS-CoV-2 spike mutations that attenuate monoclonal and serum antibody neutralization. *Cell Host Microbe* **29**, 477–488 (2021).
- Chen, R. E. et al. Resistance of SARS-CoV-2 variants to neutralization by monoclonal and serum-derived polyclonal antibodies. *Nat. Med.* **27**, 717–726 (2021).
- García-Beltrán, W. F. et al. Multiple SARS-CoV-2 variants escape neutralization by vaccine-induced humoral immunity. *Cell* **184**, 2372–2383 (2021).
- Gupta, R. K. Will SARS-CoV-2 variants of concern affect the promise of vaccines? *Nat. Rev. Immunol.* **21**, 340–341 (2021).
- Kannan, S., Shaik Syed Ali, P. & Sheeza, A. Evolving biothreat of variant SARS-CoV-2—molecular properties, virulence and epidemiology. *Eur. Rev. Med. Pharmacol. Sci.* **25**, 4405–4412 (2021).
- Bal, A. et al. Two-step strategy for the identification of SARS-CoV-2 variant of concern 202012/01 and other variants with spike deletion H69-V70, France, August to December 2020. *Eur. Surveill.* **26**, 2100008 (2021).
- Wang, P. F. et al. Antibody resistance of SARS-CoV-2 variants B.1.351 and B.1.1.7. *Nature* **593**, 130–135 (2021).
- Collier, D. A. et al. Sensitivity of SARS-CoV-2 B.1.1.7 to mRNA vaccine-elicited antibodies. *Nature* **593**, 136–141 (2021).
- Andreano, E. et al. SARS-CoV-2 escape from a highly neutralizing COVID-19 convalescent plasma. *Proc. Natl. Acad. Sci. USA* **118**, e2103154118 (2021).
- Madhi, S. A. et al. Efficacy of the ChAdOx1 nCoV-19 Covid-19 vaccine against the B.1.351 Variant. *N. Engl. J. Med.* **384**, 1885–1898 (2021).
- Zhou, D. et al. Evidence of escape of SARS-CoV-2 variant B.1.351 from natural and vaccine-induced sera. *Cell* **184**, 2348–2361 (2021).
- Alter, G. et al. Immunogenicity of Ad26.COV2.S vaccine against SARS-CoV-2 variants in humans. *Nature* **596**, 268–272 (2021).
- Hoffmann, M. et al. SARS-CoV-2 variants B.1.351 and P.1 escape from neutralizing antibodies. *Cell* **184**, 2384–2393 (2021).
- Planas, D. et al. Reduced sensitivity of SARS-CoV-2 variant Delta to antibody neutralization. *Nature* **596**, 276–280 (2021).
- Augusto, G. et al. In vitro data suggest that Indian variant B.1.617 of SARS-CoV-2 escapes neutralization by both receptor affinity and immune evasion. *Allergy* <https://doi.org/10.1111/all.15065> (2021).
- Liu, C. et al. Reduced neutralization of SARS-CoV-2 B.1.617 by vaccine and convalescent serum. *Cell* **184**, 4220–4236 (2021).
- Padilla-Rojas, C. et al. Genomic analysis reveals a rapid spread and predominance of lambda (C.37) SARS-CoV-2 lineage in Peru despite circulation of variants of concern. *J. Med. Virol.* <https://doi.org/10.1002/jmv.27261> (2021).
- Laiton-Donato, K. et al. Characterization of the emerging B.1.621 variant of interest of SARS-CoV-2. *Infect. Genet. Evol.* **95**, 105038 (2021).
- Gomez, C. E., Perdiguero, B. & Esteban, M. Emerging SARS-CoV-2 variants and impact in global vaccination programs against SARS-CoV-2/COVID-19. *Vaccines* <https://doi.org/10.3390/vaccines9030243> (2021).
- Harvey, W. T. et al. SARS-CoV-2 variants, spike mutations and immune escape. *Nat. Rev. Microbiol.* **19**, 409–424 (2021).
- Yuan, M. et al. Structural basis of a shared antibody response to SARS-CoV-2. *Science* **369**, 1119–1123 (2020).
- Toelzer, C. et al. Free fatty acid binding pocket in the locked structure of SARS-CoV-2 spike protein. *Science* **370**, 725–730 (2020).
- Walls, A. C. et al. Structure, function, and antigenicity of the SARS-CoV-2 spike glycoprotein. *Cell* **181**, 281–292 (2020).
- Cai, Y. F. et al. Structural basis for enhanced infectivity and immune evasion of SARS-CoV-2 variants. *Science* **373**, 642–648 (2021).
- Liu, Y. & Rocklöv, J. The reproductive number of the Delta variant of SARS-CoV-2 is far higher compared to the ancestral SARS-CoV-2 virus. *J. Travel. Med.* <https://doi.org/10.1093/jtm/taab124> (2021).
- Hoffmann, M. et al. SARS-CoV-2 variant B.1.617 is resistant to bamlanivimab and evades antibodies induced by infection and vaccination. *Cell. Rep.* **36**, 109415 (2021).
- Lopez Bernal, J. et al. Effectiveness of covid-19 vaccines against the B.1.617.2 (Delta) variant. *N. Engl. J. Med.* **385**, 585–594 (2021).
- Hsieh, C. L. et al. Structure-based design of prefusion-stabilized SARS-CoV-2 spikes. *Science* **369**, 1501–1505 (2020).
- Lei, J. & Frank, J. Automated acquisition of cryo-electron micrographs for single particle reconstruction on an FEI Tecnai electron microscope. *J. Struct. Biol.* **150**, 69–80 (2005).
- Zheng, S. Q. et al. MotionCor2: anisotropic correction of beam-induced motion for improved cryo-electron microscopy. *Nat. Methods* **14**, 331–332 (2017).
- Grant, T. & Grigorieff, N. Measuring the optimal exposure for single particle cryo-EM using a 2.6 angstrom reconstruction of rotavirus VP6. *Elife* **4**, e06980 (2015).
- Zhang, K. Gctf: real-time CTF determination and correction. *J. Struct. Biol.* **193**, 1–12 (2016).
- Zivanov, J. et al. New tools for automated high-resolution cryo-EM structure determination in RELION-3. *Elife* **7**, e42166 (2018).
- Kimanius, D., Forsberg, B. & Lindahl, E. Accelerated Cryo-EM structure determination with parallelisation using GPUs in relion-2. *Elife* **5**, e18722 (2016).
- Scheres, S. H. W. RELION: implementation of a Bayesian approach to cryo-EM structure determination. *J. Struct. Biol.* **180**, 519–530 (2012).
- Scheres, S. H. W. A Bayesian view on Cryo-EM structure determination. *J. Mol. Biol.* **415**, 406–418 (2012).
- Punjani, A., Rubinstein, J. L., Fleet, D. J. & Brubaker, M. A. cryoSPARC: algorithms for rapid unsupervised cryo-EM structure determination. *Nat. Methods* **14**, 290–296 (2017).
- Rosenthal, P. B. & Henderson, R. Optimal determination of particle orientation, absolute hand, and contrast loss in single-particle electron cryomicroscopy. *J. Mol. Biol.* **333**, 721–745 (2003).
- Chen, S. X. et al. High-resolution noise substitution to measure overfitting and validate resolution in 3D structure determination by single particle electron cryomicroscopy. *Ultramicroscopy* **135**, 24–35 (2013).
- Trabuco, L. G., Villa, E., Mitra, K., Frank, J. & Schulten, K. Flexible fitting of atomic structures into electron microscopy maps using molecular dynamics. *Structure* **16**, 673–683 (2008).
- Winn, M. D. et al. Overview of the CCP4 suite and current developments. *Acta Crystallogr. D* **67**, 235–242 (2011).
- Emsley, P., Lohkamp, B., Scott, W. G. & Cowtan, K. Features and development of Coot. *Acta Crystallogr. D* **66**, 486–501 (2010).
- Adams, P. D. et al. PHENIX: a comprehensive Python-based system for macromolecular structure solution. *Acta Crystallogr. D* **66**, 213–221 (2010).